Radiat Environ Biophys (2013) 52:123–133
DOI 10.1007/s00411-012-0450-9

ORIGINAL PAPER

Reduced side effects by proton microchannel radiotherapy: study in a human skin model

Olga Zlobinskaya · Stefanie Girst · Christoph Greubel · Volker Hable · Christian Siebenwirth · Dietrich W. M. Walsh · Gabriele Multhoff · Jan J. Wilkens · Thomas E. Schmid · Günther Dollinger

Received: 15 November 2012 / Accepted: 13 December 2012 / Published online: 28 December 2012
© Springer-Verlag Berlin Heidelberg 2012

Abstract The application of a microchannel proton irradiation was compared to homogeneous irradiation in a three-dimensional human skin model. The goal is to minimize the risk of normal tissue damage by microchannel irradiation, while preserving local tumor control through a homogeneous irradiation of the tumor that is achieved because of beam widening with increasing track length. 20 MeV protons were administered to the skin models in 10- or 50-μm-wide irradiation channels on a quadratic raster with distances of 500 μm between each channel (center to center) applying an average dose of 2 Gy. For comparison, other samples were irradiated homogeneously at the same average dose. Normal tissue viability was significantly enhanced after microchannel proton irradiation compared to homogeneous irradiation. Levels of inflammatory parameters, such as Interleukin-6, TGF-Beta, and Pro-MMP1, were significantly lower in the supernatant of the human skin tissue after microchannel irradiation than after homogeneous irradiation. The genetic damage as determined by the measurement of micronuclei in keratinocytes also differed significantly. This difference was quantified via dose modification factors (DMF) describing the effect of each irradiation mode relative to homogeneous X-ray irradiation, so that the DMF of 1.21 ± 0.20 after homogeneous proton irradiation was reduced to 0.23 ± 0.11 and 0.40 ± 0.12 after microchannel irradiation using 10- and 50-μm-wide channels, respectively. Our data indicate that proton microchannel irradiation maintains cell viability while significantly reducing inflammatory responses and genetic damage compared to homogeneous irradiation, and thus might improve protection of normal tissue after irradiation.

Keywords Radiation therapy · Particle therapy · Microbeam · Micronuclei · Inflammatory markers · Spatial fractionation

Introduction

Radiotherapy is accepted worldwide as one of the key modalities to treat solid tumors. The major goal of curative radiation therapy is to deliver a lethal dose to the tumor without inducing severe treatment complications in the surrounding normal tissue. Proton and ion irradiation protocols are superior to X-ray-based therapeutic approaches in terms of delivering the dose required for tumor control and at the same time minimizing the total energy deposition into the normal tissue (Durante and Loeffler 2010).

Here, we propose a novel strategy to reduce the known side effects of radiotherapy by using proton microchannel irradiation. This approach resembles earlier studies of grid or sieve therapy with X-rays (Sakka and Kamata 1958), electrons (Albert et al. 1967), and protons (Burns et al.

Olga Zlobinskaya and Stefanie Girst contributed equally to this work.

O. Zlobinskaya · D. W. M. Walsh · G. Multhoff · J. J. Wilkens · T. E. Schmid
Department of Radiation Oncology, Klinikum rechts der Isar, Technische Universität München, Munich, Germany

S. Girst (✉) · C. Greubel · V. Hable · C. Siebenwirth · G. Dollinger
Institut für Angewandte Physik und Messtechnik (LRT2), Universität der Bundeswehr München, 85579 Neubiberg, Germany
e-mail: stefanie.girst@unibw.de

G. Multhoff
Clinical Cooperation Group (CCG) "Innate Immunity in Tumor Biology", Helmholtz Zentrum München, Munich, Germany

1972) in reducing side effects in the normal tissue by sparing large parts of it from radiation ("spatial fractionation"). In the context of synchrotron-generated X-rays, this strategy is also referred to as microbeam radiation therapy (MRT; Serduc et al. 2008a). X-ray MRT, which was initially invented for radiosurgery of brain tumors in rodents at the Brookhaven National Laboratory (New York, USA) and further developed at the European Synchrotron Radiation Facility (ESRF) in Grenoble, France (Laissue et al. 2007; Brauer-Krisch et al. 2003; Brauer-Krisch et al. 2005), has been used in many more neurosurgical animal studies (Anschel et al. 2010) and was even suggested as radiation therapy method for patients (Slatkin et al. 1994). In X-ray MRT, the channel/microarray geometry is maintained in the (deep-seated) tumor. The tumors are exposed to one (unidirectional irradiation) or two (bidirectional irradiation) arrays with a thickness of a few tens of microns, consisting of parallel beams which are separated by regular distances of 50–400 μm. This irradiation geometry prevents normal brain tissue necrosis mainly through sparing of normal brain vessels (Serduc et al. 2008a, b). In spite of the spatial fractionation, tumors are controlled efficiently, presumably due to decreased blood vessel density in tumors (Griffin et al. 2012).

The main difference to X-ray MRT in our strategy is that due to proton beam scattering, a homogeneous dose distribution is generated inside the tumor, while the concept of spatial fractionation is maintained in the irradiated regions close to the skin. Proton MRT keeps the well-established advantages of tumor control by a homogeneous tumor dose when the channels widen to a homogeneous distribution within the tumor. A potential advantage of targeting the tumor volume homogeneously with dose was also recognized when it was suggested to use mircroarray X-ray fields from more directions (Dilmanian et al. 2006; Slatkin et al. 1994). However, the non-irradiated area would only cover less than 50 % of the total treated area in a two-directional case. MRT has also been proposed for heavy ions (Dilmanian and Meek 2010), but the use of protons for MRT was dismissed due to the beam widening in tissue, what we however consider an advantage.

Here, we introduce the application of micrometer-sized proton beams in radiotherapy. This approach may also be applicable for micrometer-sized beams of heavy ions such as carbon ions. Proton microchannel irradiation resembles conventional beam scanning techniques, where the tumor is conformally irradiated using a millimeter-sized pencil beam that is scanned on a rectangular grid. The pencil beam is characterized by a two-dimensional Gaussian profile for the lateral dose distribution with SD σ, commonly being called beam radius.

$$I(x,y) \propto \frac{1}{2\pi\sigma^2}\exp\left(-\frac{x^2+y^2}{2\sigma^2}\right)$$

In the conventional proton scanning scheme, the center-to-center distance d between two adjacent points is typically chosen to be smaller than twice the radius of the pencil beam resulting in a nearly homogeneous dose distribution in the tumor, but also in the skin of the patient. Figure 1a shows a treatment plan for a $3 \times 3 \times 5$ cm^3 tumor situated 10 cm beneath the skin using 144 pencil beams in a matrix with distances $d = 3.6$ mm and $\sigma = 1.8$ mm. The main difference of the proposed proton microchannel irradiation, compared to traditional methods, is that the radius of the proton beam is in the micrometer range while keeping millimeter distances d between two adjacent irradiation points as in conventional scanning modes (Fig. 1b). The radius of the microbeam may be chosen within a range of 50–500 μm and the point-to-point distance d is kept at least 10 times larger than the beam radius. Due to small angle scattering of protons and initial beam divergence, the beam spreads laterally when passing through normal tissue and becomes wider at the depth of the tumor. As an example, the beam radius is chosen as 250 μm which is less than 1/10 of the point-to-point distance of 3.6 mm of the scanning matrix (Fig. 1b). The distance is chosen to obtain dose fluctuations lower than 5 % within the tumor if no other beam divergence is assumed. The point-to-point distance could be enlarged even more when introducing additional beam divergence that results in a larger beam at the tumor site. The number of protons applied to one point of the matrix is equivalent to the number of protons that should be used with a larger pencil beam applied on the same matrix. By using this approach, the tumor will be irradiated homogeneously with the same average dose that is reached with a scanned pencil beam (Fig. 1a, b). However, within the normal tissue, an inhomogeneous dose distribution is achieved by the application of microchannel irradiation (different tissue/bone densities need to be considered in more complex models). In the skin and close to it, major parts of the tissue receive almost no dose (Fig. 1c). Simulations showed that the channel width could be further reduced (if technically feasible) in order to spare larger parts of the skin while the dose in the tumor remained homogeneous. An inhomogeneous dose distribution within normal tissues is meant to reduce normal tissue toxicity, caused by the induction of inflammatory mediators and DNA damage responses, as only a small fraction (for instance less than 1 %) of the cells in the skin receive a high dose (dose–volume effect, (Withers et al. 1988)). Due to the nature of the highly focused beam, small areas of normal tissue within the irradiated channels will receive much higher doses than the mean tumor dose. This will cause high cell

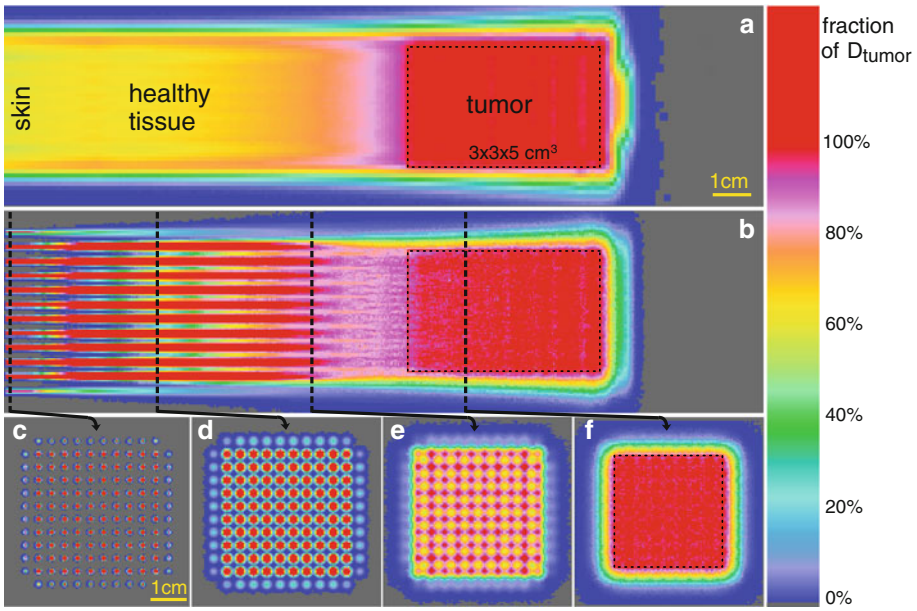

Fig. 1 Dose distributions for homogeneous and microchannel proton irradiation. The tumor is situated at 10.6–15.6 cm depth and is irradiated homogeneously with a dose D_{tumor} (=100 % on the *color bar*) by homogeneous (**a**) or microchannel (**b**) proton irradiation from one direction (beams from the *left*). The microbeams with an initial radius $\sigma_0 = 250$ μm are arranged on a *rectangular grid* with point-to-point distance $d = 3.6$ mm. The dose in the channels exceeds the tumor dose, with a skin dose in the channels of approximately 20 times that of the tumor dose (doses $\geq D_{\text{tumor}}$ are red on the color bar). However, the gray area between the microbeams does not receive any dose at all. Lateral dose distributions are shown for the skin (**c**), at 4 cm depth (**d**), 8 cm depth (**e**), and in the tumor (**f**). The dose distributions were calculated with the open-source planning system CERR (Deasy et al. 2003) and an additional proton dose algorithm (Schell and Wilkens 2010) based on Monte Carlo-generated pencil beams

death rates along the microchannels. Since the fraction of normal tissue irradiated with very high doses is very small and the surrounding cells are not hit by the beam, the overall damage within the normal tissue is expected to be significantly smaller. It is important to note that the migration of viable cells from the borders of the irradiated site could be of significance when small areas of the skin are exposed. Thus, acute reactions of the normal tissue will be reduced in comparison with broad beam or normal pencil beam irradiation. Due to the smoother lateral dose distribution, the normal tissue toxicity increases with tissue depth. In addition, the bystander effect should be taken into consideration (Belyakov et al. 2005; Sedelnikova et al. 2007; Dickey et al. 2011) that may somehow reduce the tissue sparing effect.

Close to the tumor, the dose distribution is almost homogeneous and thus no difference in tissue reaction in this part of the normal tissue as well as in the tumor is expected in relation to conventional proton irradiation conditions (Fig. 1c–f). If tumors are irradiated from two opposite directions, some inhomogeneous dose distribution, and thus tissue sparing effect, can even be retained in the normal tissue close to the tumor because the point-to-point distance of the irradiation matrix can be extended by a factor $\sqrt{2}$ without disturbing the homogeneous dose distribution within the tumor and because the protons from each side are stopped within the tumor.

For microchannel irradiation, improved transversal and longitudinal beam brightness is necessary. These technical requirements could probably be provided by modern accelerators (synchrotrons rather than cyclotrons) which are suitable for proton radiation therapy or would be a future perspective for the high brightness beams from laser-based particle accelerators. In addition, a versatile beam focusing system has to be installed to form the micrometer-sized or at least submillimeter beams. The exit nozzle between the beam transport vacuum and the ambient atmosphere has to be placed close to the patient in order to avoid a lateral spread of the beam before entering the tissue.

In order to prove the hypothesis of reduced side effects in normal tissue through microchannel proton irradiation, we report on a comparative study of microchannel and broad beam irradiation of artificial skin tissue. Our investigations were carried out in a human tissue model (3D human reconstructed skin) in order to account for the preserved three-dimensional geometric arrangement and communication of cells present in tissues in vivo. The in vitro skin model (EpiDermFT$^{\text{TM}}$, MatTek Corporation) has been used for assessing the micronucleus induction as a

skin-based genotoxicity assay (Curren et al. 2006). Meanwhile, this assay has been established to characterize different genotoxins including proton and X-ray radiation (Schmid et al. 2010; Mun et al. 2009; Hu et al. 2009). By using EpiDermFT^{TM} for radiation research with a microbeam, the group of Belyakov detected the induction of micronucleated and apoptotic cells within the ionizing track and up to 1 mm beyond (Belyakov et al. 2005).

EpiDermFT^{TM} was also used for the evaluation of the inflammatory response in skin by measuring Interleukin-6 (IL-6) levels in the media (Weindl et al. 2011). A common side effect of radiotherapy is the development of skin reactions at the irradiated area (Salvo et al. 2010). Some of these reactions are mild and immediate, while others may occur several weeks later (Porock and Kristjanson 1999). Acute radiodermatitis appears generally within 24 h after a radiation dose of 2 Gy or greater (Porock and Kristjanson 1999). It has been shown that interleukins and chemokines play an important role in the inflammatory response after irradiation (Liu et al. 2006). However, it is known that radiation-induced increases in pro-inflammatory cytokines may have deleterious effects (Sepah and Bower 2009). For example, elevated levels of interleukins are under investigation as biomarkers for the development of radiation pneumonitis in lung cancer patients (Arpin et al. 2009). It was also shown that elevated levels of pro-inflammatory cytokines for longer periods of time might be an indicator for chronic inflammation (Bower et al. 2009; Sepah and Bower 2009). Nevertheless, long-term skin effects after more than 3 weeks such as moist desquamation cannot be examined in this skin model due to its limited life span. The assessment of long-term radiation effects and of the role of blood vessels and hair follicles in the dermis (not present in EpiDermFT^{TM}), as well as the impact of the immune system after irradiation will require animal models (Rothkamm et al. 2012).

Materials and methods

Tissue construct

The three-dimensional full-thickness human skin model (EFT400; EpiDermFT^{TM}) was obtained from MatTek Corporation, Ashland, MA, USA. This human reconstructed skin is a multilayered, differentiated tissue consisting of basal, spinous, granular, and cornified layers resembling the normal human epidermis as well as a dermal layer. The tissue consists of normal, human-derived epidermal keratinocytes and dermal fibroblasts, which have been cultured on special cell culture inserts. The surface area of each tissue was 1 cm^2. Upon arrival, the EpiDermFT^{TM} tissue, supplied with New Maintenance Medium (NMM), was transferred to the wells of 12-well plates, each containing 2.0 ml of fresh 37 °C NMM. The plates were then incubated at 37 °C in a humidified atmosphere of 5 % CO_2. The culture medium was replaced every 24 h.

Irradiation conditions

Irradiation of the human tissue model using 20 MeV protons was carried out at the Munich ion microprobe SNAKE (Superconducting Nanoprobe for Applied nuclear [Kern] physics Experiments) of the 14 MV Munich tandem accelerator which has been adopted for use in biological analysis (Hauptner et al. 2004). The setup, which allows the irradiation of defined cell nuclei with single or counted protons, has already been described in detail (Greubel et al. 2008; Schmid et al. 2010). Irradiations of the skin construct were carried out in specially developed containers for biological tissue samples. A detailed description of the construction of the irradiation containers for cell irradiation has been given previously (Schmid et al. 2010). In brief, irradiation containers were built by stretching and clamping a 6-μm Mylar foil between two stainless steel plates. The EpiDermFT^{TM} tissue to be irradiated was placed on this carrier foil, and each container was covered with a second 6-μm Mylar foil. During irradiation, the container with the attached dermis was mounted directly behind the beam exit nozzle. Each proton traversing the skin was detected using a scintillator-photomultiplier detector allowing a precise dose calculation from the number of protons applied to a specific area on the tissue and the LET value (2.66 keV/μm at the skin sample).

The irradiation setup was used to prepare the beam for two focused modes (channel modes) and also for homogeneously applied protons, compensating potential systematic errors by direct comparison of the results from the different modes. In detail, we used 79,069,112 counted protons within a (close to) circular area of 16.75 mm^2 resulting in a mean dose of 2 Gy in any proton irradiation mode. The dose uncertainty of approximately 4 % is mainly given by the uncertainty of the field size ($\sim$2 % in each dimension) and the accuracy of the LET value ($\sim$1–2 %, ICRU 1993 report 49). Furthermore, there is a small contribution from the uncertainty of the number of applied protons due to pileup events in the scintillator detector situated behind the artificial skin sample (<0.5 %) and from protons scattered to larger angles within the skin tissue so that they did not reach the detector (<0.01 %).

The microchannel irradiation of the EpiDermFT^{TM} tissue was performed using 67 square channels. In each channel, 1,180,136 protons were applied. The 10 × 10 μm^2 small channels (SC) resulted in a local dose of 5,000 Gy within the channel and the 50 × 50 μm^2 large channels (LC) in 200 Gy. The distances between the channels were 500 μm

(center to center) in both cases. Three skin samples were treated for each irradiation mode, and the whole experiment was performed in duplicate.

In order to obtain a reference dose–response curve for micronuclei induction, EpiDermFT^{TM} tissue was irradiated with doses in the range of 0–4 Gy with 200 kV X-rays (RS225, XStrahl, Surrey, United Kingdom) with a dose rate of 0.88 Gy/min (15 mA, 0.8 mm Be, and 0.5 mm Cu filter) and a source–skin distance of 50 cm using a field of 20 cm × 20 cm (accuracy of delivered dose ~4 %).

MTT tissue viability test

The MTT assay (MTT-100, MatTek Corporation) was carried out as per manufacturer's instructions (Kidd et al. 2007). The MTT test is a colorimetric assay for measuring the metabolic activity of enzymes in the cell, which reduce MTT to formazan dyes, giving a purple color. In brief, 48 h after irradiation, tissues were washed twice with PBS and the central part of the irradiated area was cut out using a 3-mm biopsy and placed in fresh 6-well plates containing 300 µl/well of MTT solution. After 3 h of incubation at 37 °C, each tissue was transferred into a fresh 6-well plate with 2 ml/well of extraction solution. The plates were covered to reduce evaporation. After overnight extraction at room temperature, tissues were discarded and the contents of each well were mixed thoroughly before transferring 200 µl of the sample into 96-well plates. The optical density (OD) of the samples was read at 570 nm using a photospectrometer. Background readings at 650 nm were subtracted to obtain the correct OD. The percentage viability was determined for each tissue.

Micronuclei test

Micronuclei analysis was performed as described by Schmid (Schmid et al. 2010). Immediately after irradiation, 3 µg/ml cytochalasin B was added into the culture medium and the cultures were incubated for a further 48 h at 37 °C in a humidified atmosphere of 5 % CO_2 in air. Tissues were separated manually from the supporting membrane and then the dermis was separated from the keratinocyte-containing epidermis. For the trypsinization step, each tissue was placed in 1 ml trypsin/EDTA for 20 min at 37 °C. After hypotonic treatment using 75 mM KCL (potassium chloride) for 3 min, the keratinocytes were fixed in methanol/acetic acid (3:1) and the cell suspension was stored at 2–8 °C for at least 72 h. Microscope slides were prepared by dropping cell solutions onto clean slides and allowing them to dry. Cells were stained with acridine orange (20 µg/ml). Based on the cytokinesis block (CB), the frequency of MN could be detected precisely in the first division cycle after irradiation and easily identified from their binucleate appearance. From each sample, 500 binucleated CB cells with well-preserved cytoplasm were analyzed for the three proton irradiation modes and for X-ray irradiation. The number of MN was only counted in binucleated CB cells containing detached MN in the cytoplasm. No assays were undertaken in dermal fibroblasts because of their low density. For the determination of dose modification factors (DMF), dose–response curves of reference radiation (200 kV X-rays) were used. The DMF is defined as the ratio of the dose of the reference radiation (homogeneous exposure with 200 kV X-rays) to the applied mean proton dose using either homogeneous or inhomogeneous delivery necessary to induce the same effect. The necessary dose of reference radiation is determined by inverting the fitted dose–effect curve. As the fit parameters are highly correlated for the calculation of DMF errors, not only the diagonal elements of the covariance matrix, the parameter errors, are taken into account but also the non-diagonal elements, describing the correlation of the parameters.

Chemokine detection in the medium

The chemokines IL-6, TGF-Beta, and Pro-MMP1, which are present in the assay medium, were measured by means of commercially available enzyme-linked immunosorbent assay kits (ELISA kits; R&D systems), following the instructions for use provided by the manufacturer. Absorbance was read at 450 nm using a microplate reader. The quantification was made on the basis of calibration curves prepared for the cytokines analyzed.

Statistics

The null hypothesis that the observed pooled MN data from the three replicates (±SE) between the different spatial irradiation modes for exposure to 20 MeV protons are not different was tested by using the z test statistics. Since the conditions for the applications of the normal probability distribution hold for these data (i.e., both sample sizes are much larger than 100 cells and the products of sample sizes and proportions are greater than five), this statistical procedure could be applied. A difference at the two-sided $P < 0.05$ was considered statistically significant.

Results

Dose distributions for microchannel irradiation

The quality of the microchannel irradiation was analyzed by radiochromic films (Gafchromic EBT2). The irradiation pattern on the Gafchromic films clearly demonstrated the channel character of the irradiation, revealing a sharp dose drop at the borders of the irradiated microchannels. In

order to investigate the valley dose between the channels in detail, we used 50 times the number of protons normally applied (i.e., $50 \times 1{,}180{,}136 = 59{,}006{,}800$) to obtain valley dose levels that lie in the sensitivity range of the Gafchromic films. Figure 2 shows the measured dose distributions. The dose drop shows a slightly smeared image which is caused by the secondary electrons produced in interactions of the protons with the film and by the limited lateral resolution of the optical readout of the Gafchromic film. The data reveal that at least 93 % of the area contains less than 1 % of the applied mean dose in the two channel irradiation modes (SC and LC). This finding indicates a valley dose of less than 0.02 Gy for 93 % of the irradiated area when irradiating the tissue samples.

MTT tissue viability assay

Cell viability of the complete cut out EpiDermFT^{TM} tissue (Ø 3 mm) was measured 40 h after irradiation by using the enzymatic, colorimetric MTT cytotoxicity assay. Pooled mean values of three independent experiments and the SE are shown in Fig. 3. For the (nearly) homogeneous irradiation mode (homogeneous field, HF), the resulting cell viability in relation to unirradiated controls was 48.5 ± 6.3 %. For microchannel irradiation, the resulting cell viability was 74.3 ± 4.1 % for the 10×10 μm^2 small channels (SC) and 92.1 ± 6.1 % for the 50×50 μm^2 large channels (LC). The resulting values for HF and SC as well as for HF and LC were significantly different ($P < 0.05$). The values of SC and LC were not significantly different. The value for the positive control, which was treated with cell membrane damaging 0.1 % Triton X-100 for 1 h, was 6.3 ± 2.2 %.

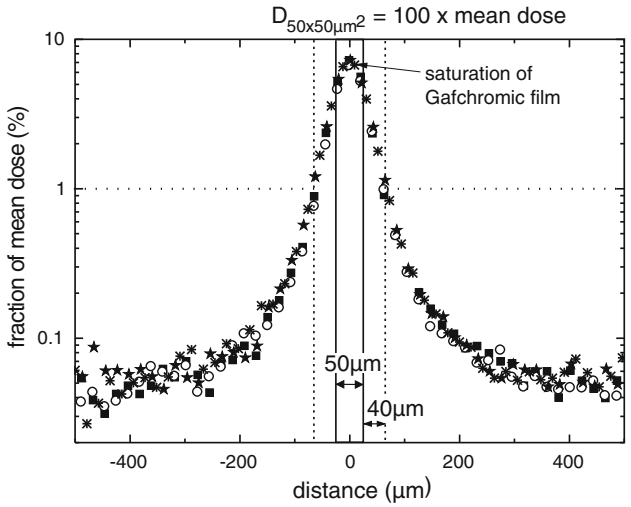

Fig. 2 Dose distribution of microchannel irradiation. Gafchromic film was irradiated on two 50×50 μm^2 fields with 59,006,800 protons, that is, 50 times the number of protons used in the experiments described in this work, to investigate valley dose distributions. *x*- and *y*-projections of the dose values of the two fields were determined and are displayed as fractions of the mean dose (i.e., the dose averaged over the total area) on a logarithmic scale (*x*: *square* and *open circle*, *y*: *stars*). The data show a dose fall-off below 1 % of the mean dose at a distance of approximately 40–50 μm from the border of the irradiated field (scanner resolution ~21 μm, film polymers ~20 μm). This means that ~93 % of the area contains less than 1 % of the dose average, thus for the performed experiments, 93 % of the irradiated tissue sample receives less than 0.02 Gy. The *arrow* indicates the saturation of the Gafchromic film within the irradiated 50×50 μm^2 field where the dose values are 100 times the mean dose

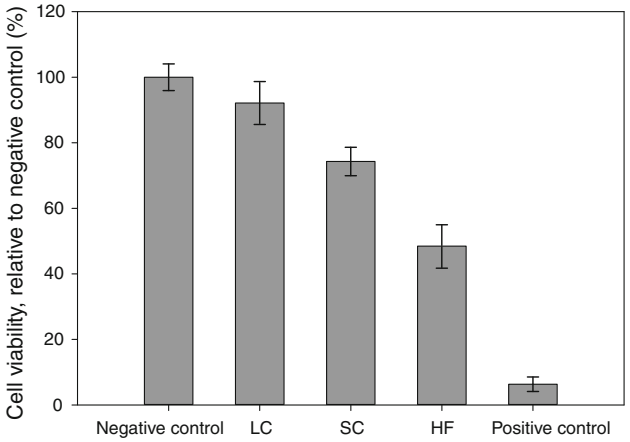

Fig. 3 MTT-test results. Cell viability of large channel (*LC*), small channel (*SC*), and homogeneous field (*HF*) irradiations was measured after 40 h by the MTT assay. *Error bars* represent the SD of the mean value of three independently irradiated EpiDermFT^{TM} tissue samples, where negative control is sham treated, unirradiated control and positive control was a tissue treated for 1 h with 0.1 % Triton. HF is significantly different ($P < 0.05$) to SC and LC

Micronuclei data

EpiDermFT^{TM} tissue was processed for micronuclei analysis as originally described by Schmid et al. (2010). The results for the induction of micronuclei (MN) and their intercellular distribution in binucleate keratinocytes from the EpiDermFT^{TM} tissue by irradiation with 200 kV X-rays are shown in Table 1 together with the corresponding control data. A weighted least-squares approximation was used to fit the data for the induction of MN in the keratinocytes with the linear function $y = c + \alpha D$. Reciprocals of the estimated variances were used as weights. The coefficients of the dose–response relationship for MN were determined as $\alpha = 0.0247 \pm 0.0020$ Gy^{-1}, $c = 0.0107 \pm 0.0021$, and the correlation coefficient between α and c to cor $(\alpha, c) = -0.535$. At all dose levels from 0 to 4 Gy, the intercellular distribution of MN is overdispersed compared to Poisson. However, there is no significant overdispersion in any irradiation mode.

Tables 2 and 3 present the corresponding results induced by 2 Gy of 20 MeV protons, which have been

Table 1 Frequency and distribution of micronuclei (MN) in cytokinesis-blocked (CB) binucleated epidermal keratinocytes from in vitro tissue induced by 200 kV X-rays

Dose (Gy)	Analyzed cells	Micronuclei per CB cell (±SE)	Intercellular distribution of micronuclei				Dispersion ratio
			0	1	2	3	σ^2/y
0	1,000	0.011 ± 0.004	991	7	2	0	1.35
0.5	1,000	0.020 ± 0.006	985	11	3	1	1.58
1	1,000	0.036 ± 0.007	971	24	3	2	1.47
2	1,000	0.069 ± 0.011	952	32	11	5	1.69
4	1,000	0.103 ± 0.013	925	55	12	8	1.60

Table 2 Frequency and distribution of micronuclei (MN) in cytokinesis-blocked (CB) binucleated epidermal keratinocytes from in vitro tissue induced by 2 Gy of 20 MeV protons at three spatial irradiation modes

ID number	Group	Analyzed cells	Micronuclei per CB cell (±SE)	Intercellular distribution of micronuclei				Dispersion ratio
				0	1	2	3	σ^2/y
1	HF	500	0.074 ± 0.016	475	16	6	3	1.74
2	HF	500	0.050 ± 0.012	480	15	5	0	1.36
3	HF	500	0.078 ± 0.016	472	20	5	3	1.64
∑1-3	HF	1,500	0.067 ± 0.009	1,427	51	16	6	1.62
4	SC	500	0.024 ± 0.009	492	5	2	1	1.81
5	SC	500	0.018 ± 0.009	495	2	2	1	2.10
6	SC	500	0.030 ± 0.011	490	7	1	2	1.91
∑4-6	SC	1,500	0.024 ± 0.006	1,477	14	5	4	1.92
7	LC	500	0.030 ± 0.010	489	7	4	0	1.51
8	LC	500	0.028 ± 0.009	489	9	1	1	1.55
9	LC	500	0.032 ± 0.012	491	4	3	2	2.10
∑7-9	LC	1,500	0.030 ± 0.006	1,469	20	8	3	1.73

Results from Experiment I

HF homogeneous field, *SC* small channels, *LC* large channels

determined at three spatial irradiation modes, each with three skin samples in two separate experiments. Since no major differences between the results of the equally irradiated samples were observed, the data of each of the experiments were pooled. These pooled data are also given as mean values in Tables 2 and 3. The mean MN data obtained in keratinocytes following exposure to 2 Gy of 20 MeV protons at the different irradiation modes are shown in Fig. 4.

The dose modification factor DMF of 20 MeV protons in the three irradiation application modes was calculated using the dose of the reference radiation 200 kV X-rays that produced a response equal to 2 Gy of protons. For the (nearly) homogeneous irradiation mode, the resulting $DMF_{HF} = 1.15 \pm 0.22$ for Experiment I and $DMF_{HF} = 1.27 \pm 0.23$ for Experiment II are equal within their SE and can thus be pooled to $DMF_{HF} = 1.21 \pm 0.20$. For microchannel irradiation within the same irradiation field, the resulting pooled DMF for the small channels was $DMF_{SC} = 0.23 \pm 0.11$ and for the large channels $DMF_{LC} = 0.40 \pm 0.12$. The resulting values of DMF_{HF} and DMF_{SC}, as well as of DMF_{HF} and DMF_{LC}, are significantly different in both experiments ($P < 0.01$). The values of DMF_{SC} and DMF_{LC} are not significantly different ($P \geq 0.05$).

Release of pro-inflammatory cytokines and chemokines

Inflammatory cytokines and chemokines were measured in the supernatant of unirradiated and irradiated EpiDermFT™ cell cultures every second day within 14 days of treatment. IL-6, TGF-Beta, and Pro-MMP1 levels were significantly higher in the supernatant of the human skin tissue after homogeneous irradiation compared to that after large and small channel application, as shown in Fig. 5. The level of Pro-MMP1 in the supernatant of the skin tissue decreased significantly faster within 14 days after irradiation with LC and SC microchannels compared to homogeneously irradiated tissues.

Table 3 Frequency and distribution of micronuclei (MN) in cytokinesis-blocked (CB) binucleated epidermal keratinocytes from in vitro tissue induced by 2 Gy of 20 MeV protons at three spatial irradiation modes

ID number	Group	Analyzed cells	Micronuclei per CB cell (±SE)	Intercellular distribution of micronuclei				Dispersion ratio
				0	1	2	3	σ^2/y
1	HF	500	0.060 ± 0.013	478	18	3	1	1.44
2	HF	500	0.088 ± 0.018	470	20	6	4	1.73
3	HF	500	0.078 ± 0.016	473	17	8	2	1.64
∑1-3	HF	1,500	0.073 ± 0.009	1,421	55	17	7	1.62
4	SC	500	0.024 ± 0.011	494	2	2	2	2.31
5	SC	500	0.018 ± 0.008	494	4	1	1	1.88
6	SC	500	0.020 ± 0.008	493	5	1	1	1.78
∑4-6	SC	1,500	0.021 ± 0.005	1,481	11	4	4	2.01
7	LC	500	0.046 ± 0.014	487	6	4	3	2.09
8	LC	500	0.032 ± 0.010	488	9	2	1	1.60
9	LC	500	0.014 ± 0.007	495	3	2	0	1.56
∑7-9	LC	1,500	0.031 ± 0.006	1,470	18	8	4	1.84

Results from Experiment II

HF homogeneous field, *SC* small channels, *LC* large channels

Discussion

The aim of the study was to introduce a new irradiation technique for radiotherapy to reduce normal tissue toxicity by sparing large areas of the normal tissue, especially close to the skin. The results presented here are also relevant for X-ray microchannel irradiation using similar beam geometries in the skin, which provided the basis for our project. In this region, the proton microchannels, which are separated by more than the channel width, are well contained, leaving the tissue in between more or less unirradiated. However, the channel width and the valley doses increase continuously with the depth of the normal tissue due to small angle scattering of the protons. This leads to a homogeneous dose distribution within the tumor if the channel diameter becomes close to or even larger than the distance of the neighboring microchannels. This holds true even if the protons are applied from one side, while tissue at the distal side is spared due to the limited proton range. Using two opposing fields or multiple fields from various directions, the channel separation can be chosen larger than twice the "channel" diameter inside the tumor because a homogeneous tumor irradiation can still be obtained through the overlap of the irradiation fields improving the normal tissue sparing effect even more.

The hypothesis of reduced adverse side effects in normal tissue through proton microchannel irradiation was proven by the comparative study with homogeneous irradiation of artificial skin tissue using the same average dose of 20 MeV protons in both cases. In our MTT and micronuclei analysis, the central part of the irradiated area was cut out and the irradiated area and the valley dose region were analyzed together. Selectively harvesting the tissue in the valley dose region only would be feasible but difficult and was not performed in this study as the total effect compared to a homogeneous irradiation was of interest.

Cell viability of the entire skin tissue measured by the MTT assay was almost unchanged compared to unirradiated controls for microchannel irradiation, while homogeneous irradiation significantly decreased tissue viability. The MTT assay is a precise measure of cell viability, because only active mitochondria are able to cleave the MTT substrate. It was previously shown that the amount of formazan generated in this enzymatic reaction correlates closely to the cell number (Berridge et al. 1996).

Potential genetic damage, quantified as micronuclei induction in skin keratinocytes, was significantly reduced for microchannel irradiation compared to homogeneous irradiation, which showed similar dose response for the induction of micronuclei as previously shown (Schmid et al. 2010). However, the DMF values of the two microchannel irradiation modes were still higher than expected, since less than 7 % of the area had been irradiated with doses larger than the average dose. A possible explanation for the higher values could be due to the bystander effect that has been demonstrated in this human tissue model (Belyakov et al. 2005; Sedelnikova et al. 2007; Dickey et al. 2011). In the study of Asur et al. (2012), bystander effects were induced using a single high dose of 10 Gy by spatially fractionation radiation treatment (Asur et al. 2012). Another study examined cell survival of cells irradiated with scattered radiation with and without intercellular communication (Butterworth et al. 2011). In this study, non-uniform dose distributions were delivered by

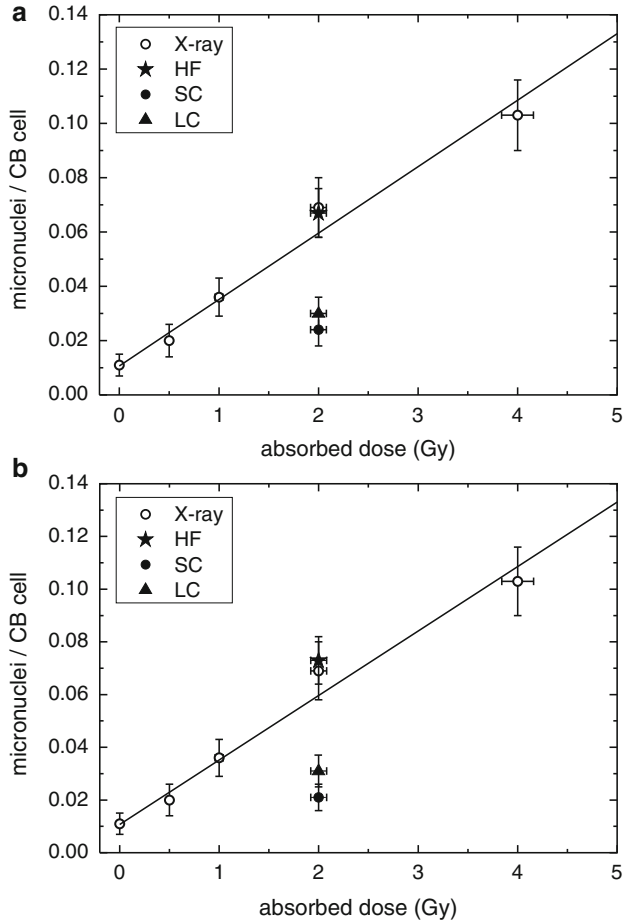

Fig. 4 Linear dose–response curve for the induction of micronuclei (*MN*) by 200 kV X-rays in cytokinesis-blocked (*CB*) binucleate keratinocytes from EpiDermFT^{TM} tissues (*open circles*). Additionally, the corresponding mean MN frequencies each determined from three single probes of exposure to 2 Gy of 20 MeV protons at differently spatial exposure conditions (HF, LC, and SC) are shown. SE of the mean are indicated by *vertical* and *horizontal error bars*. **a** Experiment I and **b** Experiment II. The same linear dose–response *curve* was used in Experiment I and II. HF is significantly different ($P < 0.01$) to SC and LC

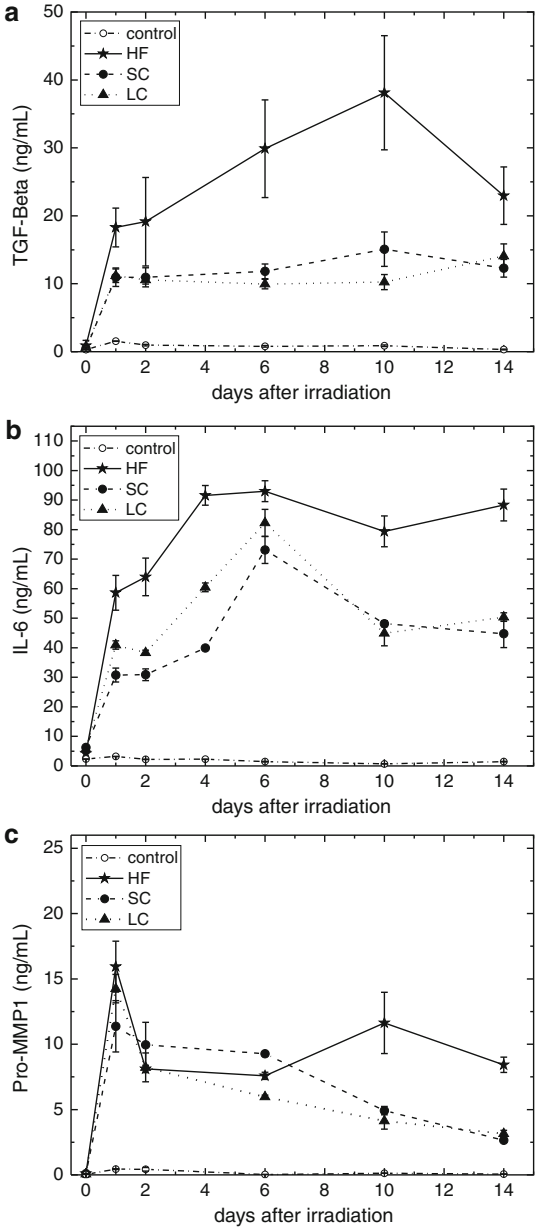

Fig. 5 Levels of TGF-Beta (**a**), Interleukin-6 (**b**), and Pro-MMP1 (**c**) in media. Changes of levels of chemokines were measured over 14 days: *HF* homogeneous field, *SC* small channels, *LC* large channels, and untreated control. SE of the mean are indicated by *vertical error bars*

shielding half of the cell population. Interestingly, cell survival was significantly lower in the shielded region. Also in this study, the authors concluded that out-of-field effects influence the clonogenic cell survival due to the occurrence of bystander effects (Butterworth et al. 2011).

A common acute adverse effect of radiotherapy is acute inflammation initiated by the irradiation of the skin. The production of pro-inflammatory cytokines and chemokines is often associated with acute adverse side effects (Fleckenstein et al. 2007; Chen et al. 2010). IL-6 is one major pro-inflammatory mediator, which is produced by keratinocytes in response to radiation (Telgenhoff and Shroot 2005; Sugawara et al. 2001). TGF-β is activated by irradiation and leads to radiation-induced fibrosis (Martin et al. 2000). TGF-β is also a predictive biomarker for radiation-induced inflammation (Martin et al. 2000). Matrix metalloproteinases (MMPs) are important regulators in the process of wound healing (Sugawara et al. 2001). Our results show that proton microchannel irradiation produces a significantly decreased inflammation response compared to the homogeneous proton irradiation. All three tested chemokines produced at the site of inflammation showed a lower increase after microchannel irradiation than after homogeneous irradiation and Pro-MMP1 levels even

decreased faster. These findings point to a decreased inflammatory response in the tissue and therefore suggest reduced acute adverse effects in radiation therapy.

We therefore hypothesize that compared to conventional homogeneous proton irradiation, irradiation with proton microchannels might reduce genotoxic effects and inflammation. Our findings point toward application of microchannel irradiation for clinical proton and/or heavy ion therapy to reduce damage of normal tissues while maintaining local tumor control via a homogeneous dose distribution within the tumor.

Acknowledgments This work was supported by the DFG-Cluster of Excellence "Munich-Centre for Advanced Photonics," and by the Maier Leibnitz Laboratory Munich. We thank Sabine Reinhardt for her support with the Gafchromic film dosimetry and Stefan Schell and Florian Kamp for their excellent technical assistance with the simulations.

References

Albert RE, Burns FJ, Heimbach RD (1967) Skin damage and tumor formation from grid and sieve patterns of electron and beta radiation in the rat. Radiat Res 30(3):525–540

Anschel DJ, Bravin A, Romanelli P (2010) Microbeam radiosurgery using synchrotron-generated submillimetric beams: a new tool for the treatment of brain disorders. Neurosurg Rev 34(2):133–142. doi:10.1007/s10143-010-0292-3

Arpin D, Mahe MA, Servois V, Claude L (2009) Predictive factors for acute radiation pneumonitis. Rev Pneumol Clin 65(3):177–186. doi:10.1016/j.pneumo.2009.03.011

Asur RS, Sharma S, Chang CW, Penagaricano J, Kommuru IM, Moros EG, Corry PM, Griffin RJ (2012) Spatially fractionated radiation induces cytotoxicity and changes in gene expression in bystander and radiation adjacent murine carcinoma cells. Radiat Res 177(6):751–765. doi:10.1667/RR2780.1

Belyakov OV, Mitchell SA, Parikh D, Randers-Pehrson G, Marino SA, Amundson SA, Geard CR, Brenner DJ (2005) Biological effects in unirradiated human tissue induced by radiation damage up to 1 mm away. Proc Natl Acad Sci USA 102(40):14203–14208. doi:10.1073/pnas.0505020102

Berridge MV, Herst PM, Tan AS (1996) The biochemical and cellular basis of cell proliferation assays that use tetrazolium salts. Biochemica 4:15–19

Bower JE, Ganz PA, Tao ML, Hu W, Belin TR, Sepah S, Cole S, Aziz N (2009) Inflammatory biomarkers and fatigue during radiation therapy for breast and prostate cancer. Clin Cancer Res 15(17):5534–5540. doi:10.1158/1078-0432.CCR-08-2584

Brauer-Krisch E, Bravin A, Lerch M, Rosenfeld A, Stepanek J, Di Michiel M, Laissue JA (2003) MOSFET dosimetry for microbeam radiation therapy at the European Synchrotron Radiation Facility. Med Phys 30(4):583–589. doi:10.1118/1.1562169

Brauer-Krisch E, Requardt H, Regnard P, Corde S, Siegbahn E, LeDuc G, Brochard T, Blattmann H, Laissue J, Bravin A (2005) New irradiation geometry for microbeam radiation therapy. Phys Med Biol 50(13):3103–3111. doi:10.1088/0031-9155/50/13/009

Burns FJ, Albert RE, Bennett P, Sinclair IP (1972) Tumor incidence in rat skin after proton irradiation in a sieve pattern. Radiat Res 50(1):181–190

Butterworth KT, McGarry CK, Trainor C, O'Sullivan JM, Hounsell AR, Prise KM (2011) Out-of-field cell survival following exposure to intensity-modulated radiation fields. Int J Radiat Oncol Biol Phys 79(5):1516–1522. doi:10.1016/j.ijrobp.2010.11.034

Chen MF, Chen WC, Lai CH, Hung CH, Liu KC, Cheng YH (2010) Predictive factors of radiation-induced skin toxicity in breast cancer patients. BMC Cancer 10:508. doi:10.1186/1471-2407-10-508

Curren RD, Mun GC, Gibson DP, Aardema MJ (2006) Development of a method for assessing micronucleus induction in a 3D human skin model (EpiDerm). Mutat Res 607(2):192–204. doi:10.1016/j.mrgentox.2006.04.016

Deasy JO, Blanco AI, Clark VH (2003) CERR: a computational environment for radiotherapy research. Med Phys 30(5):979–985

Dickey JS, Zemp FJ, Altamirano A, Sedelnikova OA, Bonner WM, Kovalchuk O (2011) H2AX phosphorylation in response to DNA double-strand break formation during bystander signalling: effect of microRNA knockdown. Radiat Prot Dosim 143(2–4):264–269. doi:10.1093/rpd/ncq470

Dilmanian AF, Meek AG (2010) Heavy Ion therapy with microbeams. US Patent 2010/0187446 A1; www.freepatentsonline.com/y2010/0187446.html

Dilmanian FA, Zhong Z, Bacarian T, Benveniste H, Romanelli P, Wang R, Welwart J, Yuasa T, Rosen EM, Anschel DJ (2006) Interlaced x-ray microplanar beams: a radiosurgery approach with clinical potential. Proc Natl Acad Sci USA 103(25):9709–9714. doi:10.1073/pnas.0603567103

Durante M, Loeffler JS (2010) Charged particles in radiation oncology. Nat Rev Clin Oncol 7(1):37–43. doi:10.1038/nrclinonc.2009.183

Fleckenstein K, Gauter-Fleckenstein B, Jackson IL, Rabbani Z, Anscher M, Vujaskovic Z (2007) Using biological markers to predict risk of radiation injury. Semin Radiat Oncol 17(2):89–98. doi:10.1016/j.semradonc.2006.11.004

Greubel C, Hable V, Drexler GA, Hauptner A, Dietzel S, Strickfaden H, Baur I, Krucken R, Cremer T, Friedl AA, Dollinger G (2008) Quantitative analysis of DNA-damage response factors after sequential ion microirradiation. Radiat Environ Biophys 47(4):415–422. doi:10.1007/s00411-008-0181-0

Griffin RJ, Koonce NA, Dings RPM, Siegel E, Moros EG, Bräuer-Krisch E, Corry PM (2012) Microbeam radiation therapy alters vascular architecture and tumor oxygenation and is enhanced by a galectin-1 targeted anti-angiogenic peptide. Radiat Res 177(6):804–812. doi:10.1667/RR2784.1

Hauptner A, Dietzel S, Drexler GA, Reichart P, Krucken R, Cremer T, Friedl AA, Dollinger G (2004) Microirradiation of cells with energetic heavy ions. Radiat Environ Biophys 42(4):237–245. doi:10.1007/s00411-003-0222-7

Hu T, Kaluzhny Y, Mun GC, Barnett B, Karetsky V, Wilt N, Klausner M, Curren RD, Aardema MJ (2009) Intralaboratory and interlaboratory evaluation of the EpiDerm 3D human reconstructed skin micronucleus (RSMN) assay. Mutat Res 673(2):100–108. doi:10.1016/j.mrgentox.2008.12.003

ICRU (1993). International commission on radiation units and measurements. ICRU Report 49, stopping powers and ranges for protons and alpha particles

Kidd DA, Johnson M, Clements J (2007) Development of an in vitro corrosion/irritation prediction assay using the EpiDerm skin model. Toxicol In Vitro 21(7):1292–1297. doi:10.1016/j.tiv.2007.08.018

Laissue JA, Blattmann H, Wagner HP, Grotzer MA, Slatkin DN (2007) Prospects for microbeam radiation therapy of brain tumours in children to reduce neurological sequelae. Dev Med Child Neurol 49(8):577–581. doi:10.1111/j.1469-8749.2007.00577.x

Liu W, Ding I, Chen K, Olschowka J, Xu J, Hu D, Morrow GR, Okunieff P (2006) Interleukin 1beta (IL1B) signaling is a critical

component of radiation-induced skin fibrosis. Radiat Res 165(2):181–191. doi:10.1667/RR3478.1

Martin M, Lefaix J, Delanian S (2000) TGF-beta1 and radiation fibrosis: a master switch and a specific therapeutic target? Int J Radiat Oncol Biol Phys 47(2):277–290

Mun GC, Aardema MJ, Hu T, Barnett B, Kaluzhny Y, Klausner M, Karetsky V, Dahl EL, Curren RD (2009) Further development of the EpiDerm 3D reconstructed human skin micronucleus (RSMN) assay. Mutat Res 673(2):92–99. doi:10.1016/j.mrgentox.2008.12.004

Porock D, Kristjanson L (1999) Skin reactions during radiotherapy for breast cancer: the use and impact of topical agents and dressings. Eur J Cancer Care 8(3):143–153

Rothkamm K, Crosbie JC, Daley F, Bourne S, Barber PR, Vojnovic B, Cann L, Rogers PA (2012) In situ biological dose mapping estimates the radiation burden delivered to 'spared' tissue between synchrotron X-ray microbeam radiotherapy tracks. PLoS ONE 7(1):e29853. doi:10.1371/journal.pone.0029853

Sakka M, Kamata R (1958) An increase in tolerance in mice by field-fractionated (sieve) x-irradiation. Radiat Res 9(3):341–345

Salvo N, Barnes E, van Draanen J, Stacey E, Mitera G, Breen D, Giotis A, Czarnota G, Pang J, De Angelis C (2010) Prophylaxis and management of acute radiation-induced skin reactions: a systematic review of the literature. Curr Oncol 17(4):94–112

Schell S, Wilkens JJ (2010) Advanced treatment planning methods for efficient radiation therapy with laser accelerated proton and ion beams. Med Phys 37(10):5330–5340. doi:10.1118/1.3491406

Schmid TE, Dollinger G, Hable V, Greubel C, Zlobinskaya O, Michalski D, Molls M, Roper B (2010) Relative biological effectiveness of pulsed and continuous 20 MeV protons for micronucleus induction in 3D human reconstructed skin tissue. Radiother Oncol 95(1):66–72. doi:10.1016/j.radonc.2010.03.010

Sedelnikova OA, Nakamura A, Kovalchuk O, Koturbash I, Mitchell SA, Marino SA, Brenner DJ, Bonner WM (2007) DNA double-strand breaks form in bystander cells after microbeam irradiation of three-dimensional human tissue models. Cancer Res 67(9):4295–4302. doi:10.1158/0008-5472.CAN-06-4442

Sepah SC, Bower JE (2009) Positive affect and inflammation during radiation treatment for breast and prostate cancer. Brain Behav Immun 23(8):1068–1072. doi:10.1016/j.bbi.2009.06.149

Serduc R, Christen T, Laissue J, Farion R, Bouchet A, Sanden B, Segebarth C, Brauer-Krisch E, Le Duc G, Bravin A, Remy C, Barbier EL (2008a) Brain tumor vessel response to synchrotron microbeam radiation therapy: a short-term in vivo study. Phys Med Biol 53(13):3609–3622. doi:10.1088/0031-9155/53/13/015

Serduc R, van de Looij Y, Francony G, Verdonck O, van der Sanden B, Laissue J, Farion R, Brauer-Krisch E, Siegbahn EA, Bravin A, Prezado Y, Segebarth C, Remy C, Lahrech H (2008b) Characterization and quantification of cerebral edema induced by synchrotron x-ray microbeam radiation therapy. Phys Med Biol 53(5):1153–1166. doi:10.1088/0031-9155/53/5/001

Slatkin DN, Spanne P, Dilmanian FA (1994) Method for microbeam radiation therapy.US patent 5339347. The United States of America. http://www.freepatentsonline.com/5339347.html

Sugawara T, Gallucci RM, Simeonova PP, Luster MI (2001) Regulation and role of interleukin 6 in wounded human epithelial keratinocytes. Cytokine 15(6):328–336. doi:10.1006/cyto.2001.0946

Telgenhoff D, Shroot B (2005) Cellular senescence mechanisms in chronic wound healing. Cell Death Differ 12(7):695–698. doi:10.1038/sj.cdd.4401632

Weindl G, Castello F, Schafer-Korting M (2011) Evaluation of anti-inflammatory and atrophogenic effects of glucocorticoids on reconstructed human skin. Altern Lab Anim 39(2):173–187

Withers HR, Taylor JM, Maciejewski B (1988) Treatment volume and tissue tolerance. Int J Radiat Oncol Biol Phys 14(4):751–759